Journal of Molecular Structure 1249 (2022) 131563

Contents lists available at ScienceDirect

Journal of Molecular Structure

journal homepage: www.elsevier.com/locate/molstr

Pure rotational spectrum and structural determination of 1,1-difluoro-1-silacyclopentane

Nicole T. Moon[a], Frank E. Marshall[a], Thomas M.C. McFadden[b], Esther J. Ocola[c], Jaan Laane[c,*], Gamil A. Guirgis[b], Garry S. Grubbs II[a,*]

[a] Missouri University of Science and Technology, 400 W 11th Street, Rolla, MO, 65409, U.S.A
[b] College of Charleston, 66 George Street, Charleston, South Carolina, 2424, U.S.A
[c] Texas A&M University, College Station, Texas, 77843, U.S.A

ARTICLE INFO

Article history:
Received 13 July 2021
Revised 17 September 2021
Accepted 22 September 2021
Available online 24 September 2021

Keywords:
Microwave Spectroscopy
CP-FTMW
Substitution Structure
Ground State Structure
1,1-difluoro-1-silacyclopentane

ABSTRACT

The ground state, pure rotational spectrum of 1,1-difluoro-1-silacyclopentane has been studied using chirped-pulse, Fourier transform microwave (CP-FTMW) spectroscopy and observed in the 6-20.3 GHz region of the electromagnetic spectrum. This spectrum was acquired leveraging the deep averaging capability of the technique. The parent species, ^{13}C, ^{29}Si, and ^{30}Si singly substituted isotopologues were observed in natural abundance and are reported. Only one conformer, the C_2 conformer (half-chair), was observed. This is confirmed with a determined CCCC dihedral angle of -48.1(11)°. The spectrum is comprised of entirely *a*-type transitions in accordance with quantum chemical calculations. Multiple split transitions are present in the spectrum which have been attributed to a ring-twisting of the carbon atoms attached to the silicon atom in the ring. This motion has the carbons crossing the *a*-axis in the *bc*-plane leading to an inversion potential. Potential energy surfaces for the ring-twisting motion were undertaken and the experimentally determined energy level difference observed in comparison to these surfaces is reasonable. A Kraitchman analysis of the experimentally determined, singly substituted isotopologues is in agreement with the optimized, twisted (nonplanar) equilibrium structure. This structure has been compared to other similar silicon-containing ring molecules using second moment arguments and these comparisons are discussed.

1. Introduction

Ever since the chirped-pulse, Fourier transform microwave (CP-FTMW) spectrometer was introduced to the scientific community over fifteen years ago [1], it has repeatedly demonstrated its advantages as a microwave technique. At the time of its debut, the main strength of the CP-FTMW was its ability to collect broadband spectra in a fraction of the time it took the traditional Balle-Flygare cavity experiment [2]. However, the Balle-Flygare cavity was still considered superior in its sensitivity. As technology has improved, however, the time advantage provided by the CP-FTMW can be leveraged to bridge the gap in sensitivity by collecting and averaging very large (100k or more) amounts of time domain molecular signals. This is known as deep averaging [1,3].

Highly accurate experimental molecular geometric structures from pure rotational spectroscopy rely heavily on the ability to collect isotopic substitution data. Ideally, this data can be collected from the molecule of study in natural abundance. For many organic molecules, the most abundant isotopologue species are ^{13}C-substituted, which are approximately 1% abundant (or some multiple of 1% depending on symmetry). Because the sensitivity in CP-FTMW spectra is traditionally lower than the Balle-Flygare FTMW instrument, collecting such data in natural abundance has been a challenge. If this barrier is overcome, though, the correct relative intensity information is useful for quick isotopologue assignment [4]. The ability to quickly average many free induction decays (FIDs) per gas pulse with very fast digitizers on broadband spectra has led to the use of deep averaging. Deep averaging makes up for the direct lack of sensitivity in the CP-FTMW technique compared to that of the cavity FTMW technique by leveraging the increased acquisition speed of the broadband spectrometer. This averaging capability – which decreases the noise floor and, thus, increases signal-to-noise (S:N) – has been utilized on the CP-FTMW instrument at the Missouri University of Science and Technology (Missouri S&T) before. The increased S:N makes it possible to garner much more information from a single broadband spectrum, particularly in regards to weaker isotopologue data [5,6]. This is espe-

* Corresponding authors.
E-mail address: ggrubbs@wesleyan.edu (G.S. Grubbs II).

https://doi.org/10.1016/j.molstruc.2021.131563
0022-2860/

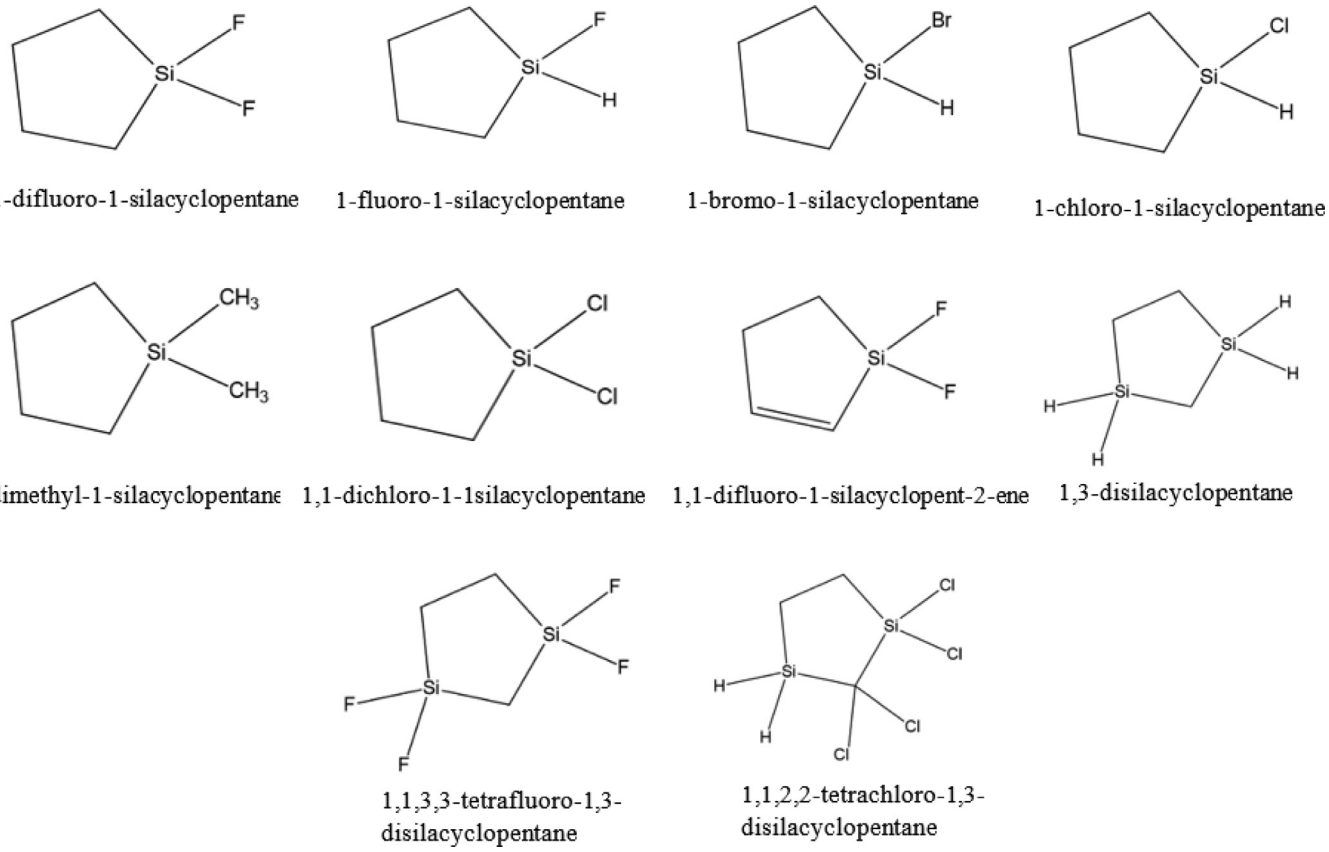

Fig. 1. Members of the silacyclopentane family previously observed.

cially useful for molecules like those of the silacyclopentane family which (a) can only be synthesized in limited quantities, (b) likely possess isotopologues that only have limited natural abundances, and (c) may possess splitting observable on only a few weaker transitions. Deep averaging, therefore, allows for a more complete understanding of a rotational spectrum of a molecular system with less sample consumption and less time.

The rotational spectrum of silacyclopentane (*c*-$C_4H_8SiH_2$) was first observed using microwave spectroscopy in 1976 [7]. At the time, only the parent and one isotopologue — the ^{29}Si isotopologue — were observed, resulting in an incomplete substitution structure. In addition, while it is generally accepted that saturated five-membered carbon rings —like that of *c*-$C_4H_8SiH_2$ — exist in a non-planar configuration due to torsional forces related to the carbon-carbon bonds [8,9], the splitting often observed in microwave spectra due to this was not reported in the original work. However, in 2011, the rotational spectrum of *c*-$C_4H_8SiH_2$ was collected again using a Balle-Flygare type, pulsed-jet Fourier transform microwave (FTMW) spectrometer as well as a CP-FTMW [10]. This work observed and reported the parent and all corresponding unique heavy atom, singly substituted isotopologues, resulting in a heavy atom structure. Since then, numerous other members of this family of molecules have been accurately studied using CP-FTMW along with IR and Raman spectroscopy including 1-fluoro-1-silacyclopentane [11], 1-bromo-1-silacyclopentane [12], 1,1-difluoro-1-silacyclopent-2-ene [13,14], 1-chloro-1-silacyclopentane [15], 1,1-dimethyl-1-silacyclopentane [16], 1,1-dichloro-1-silacyclopentane [17], 1,3-disilacyclopentane [13], 1,1,2,2-tetrachloro-1,3-disilacyclopentane [18], and 1,1,3,3-tetrafluoro-1,3-disilacyclopentane [19]. The structures of these molecules can be seen in Fig. 1.

In this work, therefore, the sensitivity advantage of CP-FTMW spectroscopy due to deep averaging is demonstrated on a member of the silacyclopentane family, 1,1-difluoro-1-silacyclopentane (*c*-$C_4H_8SiF_2$). The microwave spectrum of *c*-$C_4H_8SiF_2$ parent as well as the ^{13}C, ^{29}Si, and ^{30}Si isotopologues in natural abundance have been observed and are reported, resulting in an experimentally determined ring structure (r_s). Splitting due to ring-twisting motions in the molecule have been observed, analysed, and reported. Quantum chemical calculations were undertaken to fully interpret the observed spectra and are reported. The calculations indicate that the barrier to the ring-twisting motion is high, resulting in twisting levels in the ground state which are degenerate (or near degenerate). Observation of the ring-twisting motion splitting, therefore, is owed to the high-resolution and deep averaging capabilities of the CP-FTMW technique. Additional quantum chemical calculations were carried out on the parent *c*-$C_4H_8SiH_2$ molecule for the sake of comparison.

2. Experimental

2.1. Synthetic Work

The synthetic work was carried out at the College of Charleston in two steps. First, 1,1-dichloro-1-silacyclopentane (*c*-$C_4H_8SiCl_2$) was prepared by adding a double Grignard reagent of 1,4-dibromobutane in anhydrous ethyl ether to a solution of silicon tetrachloride in additional ethyl ether under argon. The method for the synthesis of *c*-$C_4H_8SiCl_2$ is the same as that reported by Tacke [20] and Charette [21]. The NMR data for *c*-$C_4H_8SiCl_2$ ^{1}H NMR (400 MHz, $CDCl_3$): δ (ppm) 1.47 (p, 4.32 Hz, 4H, CH_2) 0.43 (t, 1.21 Hz, 4H, CH_2). ^{13}C NMR (400 MHz, $CDCl_3$): δ (ppm) 28.88 (s), 14.70 (s). ^{29}Si NMR (400 MHz, $CDCl_3$): δ (ppm) 16.52 (s). The sample of *c*-$C_4H_8SiF_2$ was prepared by fluorination of *c*-$C_4H_8SiCl_2$ with freshly sublimed antimony trifluoride without solvent (Scheme 1).

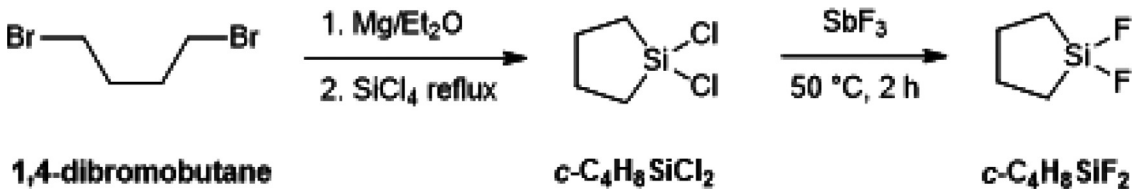

Scheme 1. Reaction conditions for the synthesis of *c*-$C_4H_8SiCl_2$ and *c*-$C_4H_8SiF_2$

The synthesis of *c*-$C_4H_8SiF_2$ has been reported previously [22], but a new procedure was developed which uses more readily available commercial compounds and it is reported below. A liquid sample of *c*-$C_4H_8SiCl_2$ (2.00 g, 16.4 mmol) was added to a 50 mL Schlenk tube, 20 cm in length, and equipped with a stir bar. The tube was fitted with a vacuum adapter and the sample with frozen with liquid nitrogen. Antimony trifluoride (3.22 g, 18.0 mmol) was added while purging with argon. The tube containing the reaction mixture was sealed, frozen with liquid nitrogen, and evacuated to 0.20 Torr. The mixture warmed to room temperature, stirred for 30 minutes, and then was heated to 50°C for two hours while stirring. Volatile components were removed from the flask using vacuum transfer and the product was purified using trap-to-trap distillation. The purity of the sample was checked using nuclear magnetic resonance spectroscopy and infrared spectroscopy. For the infrared spectrum, the SiF_2 symmetric and antisymmetric stretching frequencies were observed at 871 and 877 cm^{-1} as previously reported [14]. A total of 1.76 g, 11.5 mmol of isolated product was collected. Yield: 69 %. ^{1}H NMR (400 MHz, $CDCl_3$): δ (ppm) 1.70 (m, 1.6 Hz, 4H, CH_2) 0.72 (m, 2.9 Hz, 4H, CH_2). ^{13}C NMR (400 MHz, $CDCl_3$): δ (ppm) 23.64 (t, 2.9 Hz), 7.48 (t, 14.0 Hz). ^{19}F NMR (400 MHz, $CDCl_3$): δ (ppm) -138.59. ^{29}Si NMR (400 MHz, $CDCl_3$): δ (ppm) 18.79.

2.2. Microwave Spectra

The microwave experiments were carried out at Missouri S&T using a CP-FTMW. The details of this spectrometer are reported elsewhere [5,6,23,24]. The sample of *c*-$C_4H_8SiF_2$ — a liquid under standard conditions — was made into a gas mix by utilizing the vapor pressure of the molecule at room temperature. A gas tank was evacuated and attached to the sample, which then allowed the sample to vaporize. The vapor in the tank was then mixed with industrial grade argon gas until the sample was 3% in concentration. The 3% gas tank was then attached to the CP-FTMW, and sample was introduced at a sub-atmospheric pressure of 0.66 atm relative to vacuum.

Spectra of *c*-$C_4H_8SiF_2$ were then acquired in the 6-12 GHz and 12-18 GHz regions of the electromagnetic spectrum using 4 μs chirp widths. A Parker Hannifin® Series 9 supersonic nozzle pulsed sample into the chamber at a rate of 5 Hz with 5 FIDs per gas pulse. In total, 168,000 FIDs, each FID being 20 μS in length, were averaged together in each frequency range before the sample was completely depleted. Spectra for the 6-12 GHz and 12-18 GHz ranges can be seen in Figs. 2 and 3, respectively. Typical linewidths for the spectra were 70-80 kHz with an attributed 10 kHz uncertainty in the line centers.

3. Quantum Chemical Calculations

3.1. Structure Calculations

The geometric structure of c-$C_4H_8SiF_2$ was optimized at the B3LYP/cc-pVTZ level at Missouri S&T. The optimized structure provided the rotational constants utilized in the initial experimental analyses. In order to carry out the calculations, Gaussian09 [25] was used in conjunction with GaussView 5.0 [26] for visualizing structures. The results from this optimized equilibrium structure can be found in Table 1.

In addition, optimized geometries and conformational energies of c-$C_4H_8SiF_2$ were calculated at the MP2/cc-pVTZ and CCSD/cc-pVTZ ab initio level of theory at Texas A&M University. For these calculations, Gaussian16 [27] was used in conjunction with GaussView 6.1.1 [26] in order to visualize the structures.

The calculated geometrical structures of the molecule are shown in Fig. 4. The twisted structures have C_2 symmetry. This was the only conformer observed in the spectra.

Table 1 presents the calculated geometrical parameters of c-$C_4H_8SiF_2$ and the microwave values to be discussed within the Discussion section. Similarly, Table 2 presents the second moment values to be discussed within the Discussion section.

3.2. Kinetic Energy and Potential Energy Calculations

The one-dimensional Schrödinger equation in terms of the ring-twisting coordinate x_2 (as shown in Fig. 6) is

$$H(x_2)\Psi(x_2) = E\Psi(x_2) \quad (1)$$

where the Hamiltonian is given by

$$H(x_2) = \left(\frac{\hbar}{2}\right)\frac{\partial}{\partial x_2}g_{55}(x_2)\frac{\partial}{\partial x_2} + (x_2). \quad (2)$$

$V(x_2)$ is given in

$$V(x_2) = a{x_2}^4 + b{x_2}^2 \quad (3)$$

and the reciprocal reduced mass expansion $g_{55}(x_2)$ reflects the fact that the reduced mass value changes with the ring-twisting coordinate is given by

$$g_{44}(x_2) = \sum_{i=0}^{6} g_{55}^{(i)}{x_2}^i. \quad (4)$$

These $g_{55}(x_2)$ terms were calculated by methods previously described [29–31].

The Laane group TWISTANE program [32], which is based on vector and numerical methods, was used to calculate the coordinate dependent kinetic energy functions $g_{55}(x_2)$ for the ring-twisting. The geometrical parameters for the computed planar structures of these molecules provided the input for the programs. The vibration was assumed to be curvilinear and the magnitude of the reciprocal reduced mass g_{55} was calculated for different values of the ring-twisting coordinate x_2 so that the full $g_{55}(x_2)$ function could be determined. (Subscripts 1 to 3 on g are reserved for the molecular rotations and 4 for the ring-puckering vibration).

Using these potential energy parameters in Eq. (3), the DA1OPTN Meinander-Laane potential energy program [33] was used to calculate the theoretical energy levels and energy level spacings, seen in Fig. 9.

The theoretical equations for the 1-D potential energy functions and the calculated potential energy surface which as coordinates the ring-twisting angle, and the ring-twisting coordinate were obtained using the MAPLE 2015.1 computing environment [34].

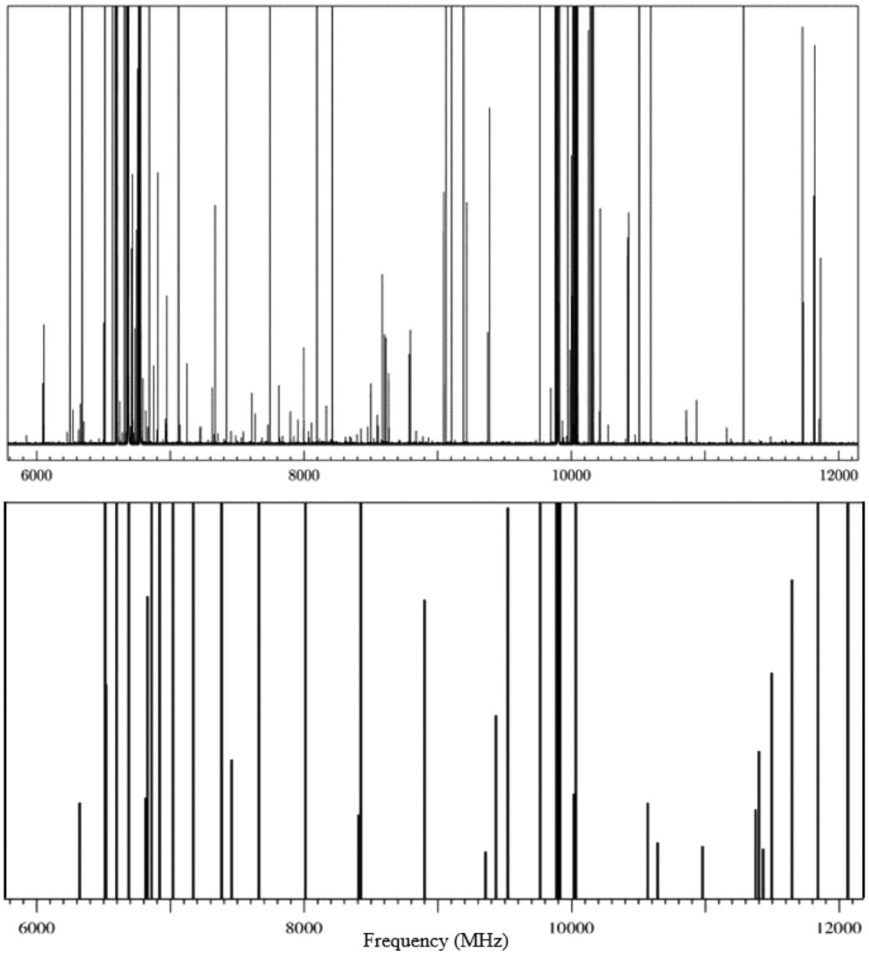

Fig. 2. The top image depicts the 6-12 GHz spectra for 1,1-difluoro-1-silacyclopentane (*c*-$C_4H_8SiF_2$). The bottom image depicts the predicted spectra within the 6-12 GHz region. Intensities of the strongest transitions are cut off so that less intense transitions are visible.

Table 1
Geometric Parameters for c-$C_4H_8SiF_2$.

	Experimental (r_s)	Theoretical (r_e)		
	microwave[a]	B3YLP/cc-pVTZ	MP2/cc-pVTZ	CCSD/cc-pVTZ
	Bond Length, Å	*Bond Length, Å*		
Si—C1	1.85(6)[b]	1.864	1.866	1.867
C1—C2	1.56(5)	1.548	1.646	1.548
Si—C4	1.85(6)	1.864	1.866	1.867
C2—C3	1.54(1)	1.542	1.537	1.540
C3—C4	1.56(5)	1.548	1.646	1.548
	Bond Angle, deg	*Bond Angle, deg*		
C1—Si—C4	99.84(44)	98.5	98.1	98.2
C2—C1—Si	101.7(26)	102.1	113.3	101.9
C3—C2—C1	109.1(30)	108.9	99.0	108.5
C4—C3—C2	109.1(30)	108.9	108.3	108.5
C4—Si—C1	99.84(44)	98.5	98.1	98.2
	Dihedral Angles, deg	*Dihedral Angles, deg*		
Si—C1—C2—C3	34.8(85)	35.6	37.8	37.0
C1—C2—C3—C4	-48.1(11)	-49.2	-52.3	-51.1
C2—C3—C4—Si	34.8(85)	35.6	37.8	37.0
C3—C4—Si—C1	-12.3(50)	-12.7	-13.4	-13.2
C4—Si—C1—C2	-12.3(50)	-12.7	-13.4	-13.4

[a] Parameters obtained through Kisiel's EVAL program [28].
[b] Uncertainties obtained from Costain errors given in values of the least significant figure.

Table 2
c-$C_4H_8SiF_2$ Second Moments from Experiment.

	Parent	^{29}Si	^{30}Si	^{13}C1 / ^{13}C4	^{13}C2 / ^{13}C3
$\boldsymbol{P_{aa}}$(amu-Å^2)	227.27110(12)	227.598(13)	227.913(11)	227.658(11)	231.1328(56)
$\boldsymbol{P_{bb}}$(amu-Å^2)	83.037692(12)	83.00(13)	83.035(11)	84.651(11)	83.6112(56)
$\boldsymbol{P_{cc}}$(amu-Å^2)	67.164670(12)	67.159(13)	67.161(11)	67.540(11)	67.1653(56)

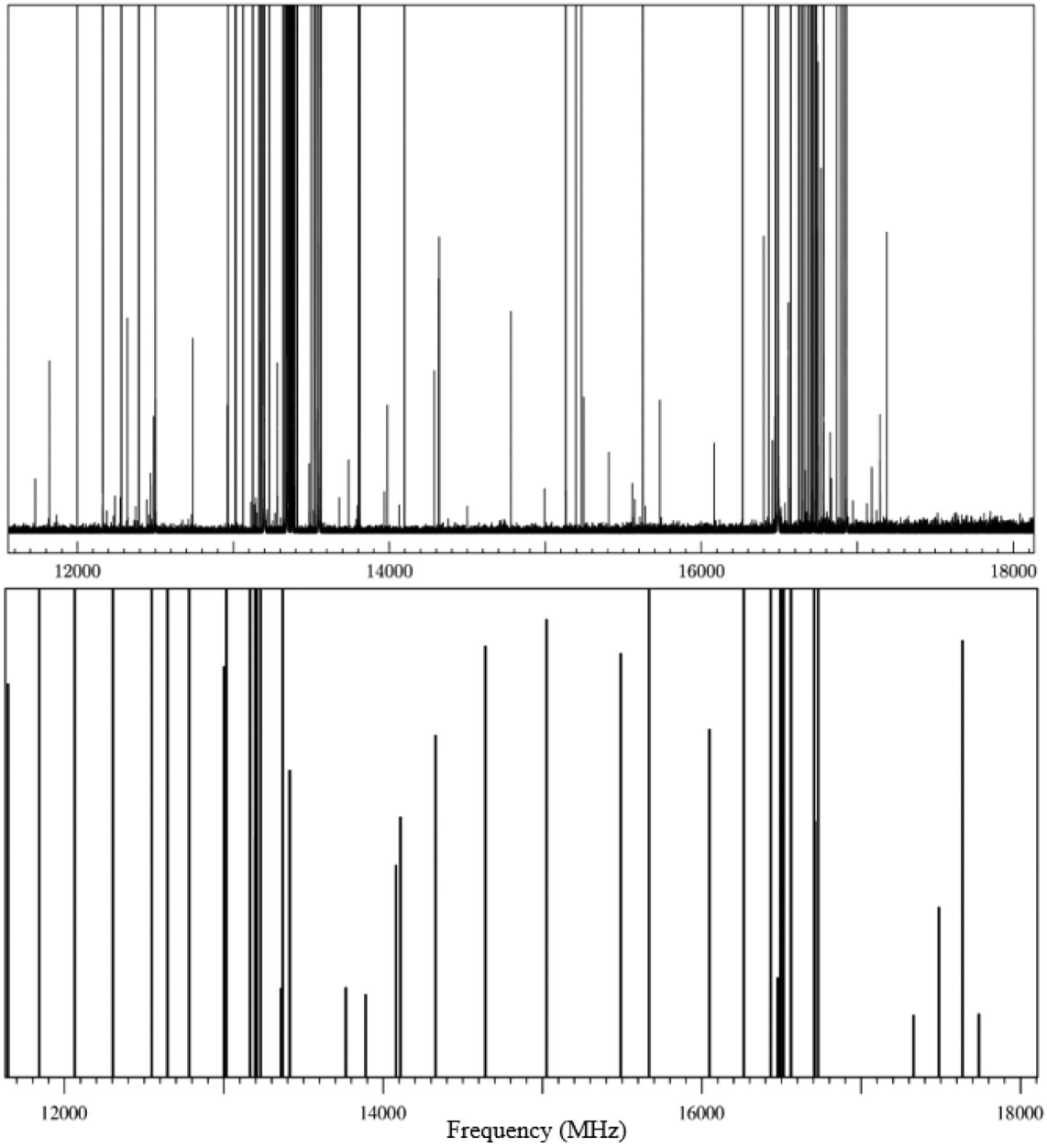

Fig. 3. The top image depicts the 12-18 GHz spectra for *c*-$C_4H_8SiF_2$. The bottom image depicts the predicted spectra within the 12-18 GHz region. Intensities of the strongest transitions are cut off so that less intense transitions are visible.

3.3. Potential Energy Surfaces

The potential energy surface (PES) based on the calculated MP2/cc-pVTZ energies of 34 different configurations calculated for *c*-$C_4H_8SiF_2$ is:

$$V(\mathrm{cm}^{-1}) = 3.297 \times 10^5 x_1^4 - 2.971 \times 10^4 x_1^2 + 4.080 \times 10^4 x_2^4 - 2.007 \times 10^4 x_2^2 + 2.854 \times 10^5 x_1^2 x_2^2 + 4.337 \times 10^3 x_1^4 x_2^4 + 2328.$$

For the sake of comparison, the potential energy surface (PES) based on the calculated MP2/cc-pVTZ energies of 28 different configurations calculated for *c*-$C_4H_8SiH_2$ is:

$$V(\mathrm{cm}^{-1}) = 3.928 \times 10^5 x_1^4 - 4.039 \times 10^4 x_1^2 + 4.433 \times 10^4 x_2^4 - 2.124 \times 10^4 x_2^2 + 2.929 \times 10^5 x_1^2 x_2^2 + 9.540 \times 10^6 x_1^4 x_2^4 + 2328.$$

The calculated PES for *c*-$C_4H_8SiF_2$ and *c*-$C_4H_8SiH_2$ and the plot of their contour maps are shown in Figs. 7 and 8.

Numerically and graphically it is seen on Table 3 and Figs. 7 and 8 that the calculated geometric parameters for the twisted conformers are quite similar for 1,1-difluorosilacyclopentane and silacyclopentane. However, the energy for the pure bent conformation for 1,1-difluorosilacyclopentane is 669 cm^{-1} lower in energy than its planar form and the pure bent conformation for silacyclopentane is 1036 cm^{-1} lower in energy that its planar form leading the visualization of this local minimum closer to the respective global maximum.

3.4. Potential Energy Functions for the Ring-Twisting

The potential energy functions (PEFs) for c-$C_4H_8SiF_2$ and c-$C_4H_8SiH_2$ were obtained according to both MP2/cc-pVTZ and CCSD/cc-pVTZ computations.

The calculated reduced mass for c-$C_4H_8SiF_2$ is 33.31 amu from the CCSD/cc-pVTZ computations and 33.41 amu from the MP2/cc-

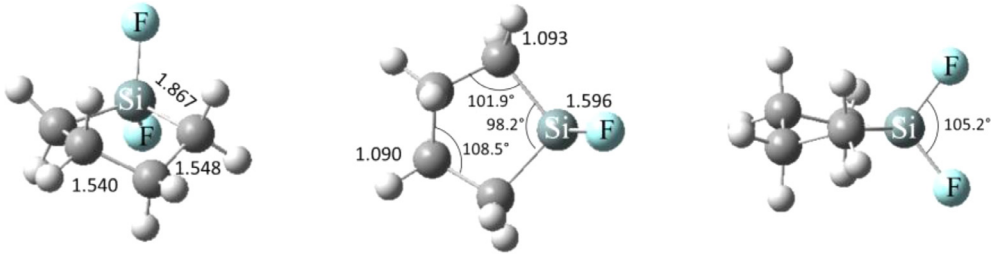

Fig. 4. Calculated geometrical parameters from CCSD/cc-pVTZ computations of the twisted conformation of *c*-$C_4H_8SiF_2$.

Table 3
Calculated energies and ring parameters of selected conformations of c-$C_4H_8SiH_2$ (top) and c-$C_4H_8SiF_2$ (bottom) at the CCSD and MP2 levels of theory.

	c-$C_4H_8SiH_2$					
	Twisted, C_2		Bent, C_s		Planar (TS)	
	CCSD/cc-pVTZ	MP2/cc-pVTZ	CCSD/cc-pVTZ	MP2/cc-pVTZ	CCSD/cc-pVTZ	MP2/cc-pVTZ
Energy, cm^{-1}	0	0	1566	1659	2136	2328
τ, radians	+/-0.48	+/-0.48	0	0	0	0
x, Å	0	0	+/-0.204	+/-0.211	0	0
	c-$C_4H_8SiF_2$					
	Twisted		Bent		Planar (TS)	
	CCSD/cc-pVTZ	MP2/cc-pVTZ	CCSD/cc-pVTZ	MP2/cc-pVTZ	CCSD/cc-pVTZ	MP2/cc-pVTZ
Energy, cm^{-1}	0	0	1451	1508	2338	2544
τ, radians	+/- 0.48	+/-0.49	0	0	0	0
x, Å	0	0	+/- 0.224	+/-0.232	0	0

pVTZ computations. The g_{55} (x) kinetic energy functions are done using the geometrical parameters of the planar structures. The g_{55} (x) kinetic energy function for c-$C_4H_8SiF_2$ from the CCSD/cc-pVTZ computations is:

$$g_{55}(x) = 3.002 \times 10^{-2} - 9.597 \times 10^{-2}x_2^2 + 3.002 \times 10^{-2}x_2^4 \quad (5)$$

and the theoretical 1-D PEF is:

$$V\left(cm^{-1}\right) = 4.199 \times 10^4 x_2^4 - 1.894 \times 10^4 x_2^2 \quad (6)$$

The g_{55} (x) kinetic energy function for *c*-$C_4H_8SiF_2$ from the MP2/cc-pVTZ computations is:

$$g_{55}\ (x) = 2.993 \times 10^{-2} - 9.638 \times 10^{-2}x_2^2 + 1.401 \times 10^{-1}x_2^4 \quad (7)$$

and the theoretical 1-D PEF is:

$$V(\mathrm{cm}-1) = 4.324 \times 10^4 x_2^4 - 2.007 \times 10^4 x_2^2. \quad (8)$$

Fig. 9 shows the calculated energy levels for *c*-$C_4H_8SiF_2$ using the g_{55} (x) functions and the calculated potential energy parameters in the DA1OPTN Meinander-Laane potential energy program [33].

Previously two-dimensional fits for the calculation of the energy levels taking in account the ring-puckering parameter, ring-puckering parameter, x_1 and the ring-twisting parameter, x_2 based on experimental data have been reported for the parent *c*-$C_4H_8SiH_2$ molecule [35]. Utilizing the calculated reduced mass and the g55 (x) values from our present work, we have calculated a one-dimensional experimentally fitted PEF that is shown in Fig. 10. Table 4 shows a comparison of the observed and calculated ring-twisting frequencies, and the agreement is very good. This PEF may be compared to the theoretically determined PEFs in Fig. 10. These are presented to provide a perspective on the accuracy that can be expected for the difluoride PEF presented in this work.

The 1990 paper [35] reported a 1-D PEF fit barrier of 3250 cm^{-1}. Our experimental 1-D barrier is 2951 cm^{-1}. The paper also shows an optimal two-dimensional fit with a barrier of 2110 cm^{-1}, which is very similar to that obtained from our theoretical CCSD/cc-pVTZ computations, which is 2338 cm^{-1}.

The experimentally 1-D PEF for *c*-$C_4H_8SiH_2$ obtained in this work is:

$$V(\mathrm{cm}-1) = 2.518 \times 10^4 x_2^4 - 1.724 \times 10^4 x_2^2. \quad (9)$$

The calculated reduced mass for the parent *c*-$C_4H_8SiH_2$ molecule is 30.17 amu according to our CCSD/cc-pVTZ computations. This calculated reduced mass along with its complete g_{55} (x) expression was used to perform the experimental fit. The value of the reduced mass from our MP2/cc-pVTZ computations is 30.19 amu. Previously the reduced mass was reported to be 31.38 amu by Laane et al in 1990 [35]. The g_{55} (x) kinetic energy function for *c*-$C_4H_8SiH_2$ from the CCSD/cc-pVTZ computations is:

$$g_{55}\ (x)\ 3.315 \times 10^{-2} - 7.484 \times 10^{-3}x_2^2 + 6.427 \times 10^{-3}x_2^4. \quad (10)$$

and the related theoretical PEF is:

$$V(\mathrm{cm}-1) = 4.199 \times 10^4 x_2^4 - 1.894 \times 10^4 x_2^2. \quad (11)$$

The g_{55} (x) kinetic energy function for *c*-$C_4H_8SiH_2$ from the MP2/cc-pVTZ computations is:

$$g_{55}\ (x) = 3.312 \times 10^{-2} - 7.460 \times 10^{-3}x_2^2 + 6.413 \times 10^{-3}x_2^4. \quad (12)$$

and the related theoretical PEF is:

$$V(\mathrm{cm}-1) = 4.433 \times 10^4 x_2^4 - 2.124 \times 10^4 x_2^2. \quad (13)$$

Fig. 11 shows the theoretical PEFs along with their calculated energy levels for the parent *c*-$C_4H_8SiH_2$ using the g_{55} (x) functions.

4. Results and Analysis

4.1. Microwave Spectra and Analysis

Analysis of the spectra was performed using SPFIT and SPCAT [36] in combination with Kisiel's AABS package [37]. An S-reduced

Table 4
Observed and Calculated Ring-Twisting Transitions (cm^{-1}) for c-$C_4H_8SiH_2$ from Experimental Fitted PEF.

	Observed[a]	Experimental fit					
	FIR	This work		Literature[a]			
Transition	V(cm^{-1})	V(cm^{-1})[b]	Δ	V(cm^{-1})[c]	Δ	V(cm^{-1})[d]	Δ
FIR[a]							
0 – 2	265.2	265.3	-0.1	265.2	0.0	267.9	-2.7
2 – 4	260.5	260.5	0.0	260.5	0.0	260.5	0.0
4 – 6	255.8	255.5	0.3	255.7	0.1	252.3	3.5
6 – 8	249.8	250.0	-0.2	250.6	0.8	243.4	6.4

[a] From reference [35].
[b] $V(cm^{-1}) = 2.518 \times 10^4 x_2^4 - 1.724 \times 10^4 x_2^2$.
[c] $V(cm^{-1}) = 2.46 \times 10^4 x_1^4 - 1.26 \times 10^4 x_1^2 + 2.28 \times 10^4 x_2^4 - 1.70 \times 10^4 x_2^2 + 9.47 \times 10^4 x_1^2 x_2^2$
[d] $V(cm^{-1}) = 1.10 \times 10^4 x_1^4 - 5.14 \times 10^3 x_1^2 + 3.68 \times 10^4 x_2^4 - 1.76 \times 10^4 x_2^2 + 1.17 \times 10^5 x_1^2 x_2^2$

Table 5
c-$C_4H_8SiF_2$ Experimental Parameters Compared to Theory (DFT).

Ground Vibrational States	c-$C_4H_8{}^{28}SiF_2$ Splitting Fit Separately	c-$C_4H_8{}^{28}SiF_2$ Splitting Fit Together	^{29}Si	^{30}Si	$^{13}C1$ / $^{13}C4$	$^{13}C2$ / $^{13}C3$
A_0 (MHz)	3364.6527(41)[a]	3364.654176(50)	3364.86(57)	3364.80(47)	3320.69(50)	3351.84(25)
B_0 (MHz)	1716.4316(12)	1716.4320798(82)	1714.5574(31)	1712.7135(30)	1712.0044(36)	1694.2075(18)
C_0 (MHz)	1628.6318(12)	1628.6325533(77)	1626.9383(31)	1625.2808(30)	1618.2019(37)	1605.6823(18)
A_1 (MHz)	3364.6453(57)	–	–	–	–	–
B_1 (MHz)	1716.4204(53)	–	–	–	–	–
C_1 (MHz)	1628.6278(45)	–	–	–	–	–
D_J (kHz)	0.145(23)	0.17637(31)	[0.17637][c]	0.122(50)	0.140(64)	0.090(31)
D_{JK} (kHz)	0.911(56)	1.00210(59)	[1.0021]	1.11(16)	1.07(20)	1.54(10)
D_K (kHz)	1.07(45)	0.6148(68)	[0.6148]	[0.6148]	[0.6148]	[0.61478]
F_{bc} (MHz)	0.930(52)	0.83595(75)	[0.83595]	[0.83595]	[0.83595]	[0.83595]
$\Delta E_{0,1}$ (MHz)	39755.59(64)	39756.547(79)	[39756.547]	[39756.547]	[39756.547]	[39756.547]
ν_{RMS} (kHz)[b]	16.6	25.3	29.7	21.4	27.7	12.9
Number of Transitions	47	47	24	24	26	22
Theoretical Equilibrium Parameters *B3LYP/cc-pVTZ*						
A_e (MHz)	3340	3340	3340	3340	3300	3330
B_e (MHz)	1700	1700	1640	1700	1700	1680
C_e (MHz)	1620	1620	1610	1610	1610	1590

[a] Numbers in parentheses give standard errors at 1σ (67% confidence) level to the least significant figure.
[b] MW RMS is defined as $\sqrt{(\sum[(obs-calc)^2]/N)}$.
[c] Values in brackets there were held to the parent value.

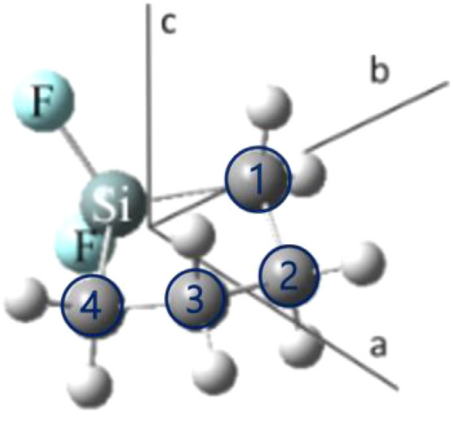

Fig. 5. Principal axes a, b, and c of the c-$C_4H_8SiF_2$ twisted structure.

Hamiltonian in the I^r representation was employed while fitting the spectra. Using the calculated rotational constants, which can be seen in Table 5, a total of 50 lines for the parent species were observed. Although the experiment was only powered for 6-18 GHz, transitions up to 20.3 GHz for the parent isotopologue were observed and assigned. Fig. 5 shows the location of the a, b, and c axes for c-$C_4H_8SiF_2$. In addition, the isotopologues corresponding to each ^{13}C, ^{29}Si, and ^{30}Si were observed and their corresponding rotational constants can be found in Table 5. For the isotopologues 26, 22, 24, and 24 transitions were observed for $^{13}C1/^{13}C4$, $^{13}C2/^{13}C3$, ^{29}Si, and ^{30}Si, respectively. It should be noted that some of the Microwave RMS values for these isotopes are larger than traditional values due to the parameters added for the splitting but are of usual magnitude for similar large amplitude motion spectroscopic fits. Table 5 also shows the calculated rotational constants from the theoretical calculations. Overall, the theoretical calculations appear to be in good agreement with the experimental data since the values differ by roughly 1%. The quantum number assignments and fits can be found in the Supporting Information.

All observed lines are a-type transitions. No b-type or c-type transitions were observed. These observations are in accordance with the predicted dipole values of 2.47, 0.00, and 0.00 D for μ_a, μ_b, and μ_c, respectively, at the B3LYP/def2TZVP with gd3bj level of theory. In addition, the majority of transitions were R-branch transitions with the second most abundant transitions being Q-branch. No P-branch transitions were observed.

As mentioned previously, splitting in the spectra due to the ring puckering motion was observed. An example of one such transition exhibiting this splitting is the $6_{06} \leftarrow 5_{05}$ transition shown in Fig. 12. Fifteen such transitions exhibited this type of splitting. Thus, to fit those transitions, a rotation-vibration term, F_aP_{apz}, was

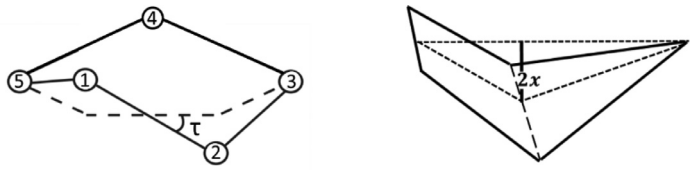

Fig. 6. Definition of the ring-twisting angle $\tau = x_2$ and the ring-puckering coordinate, $x = x_1$.

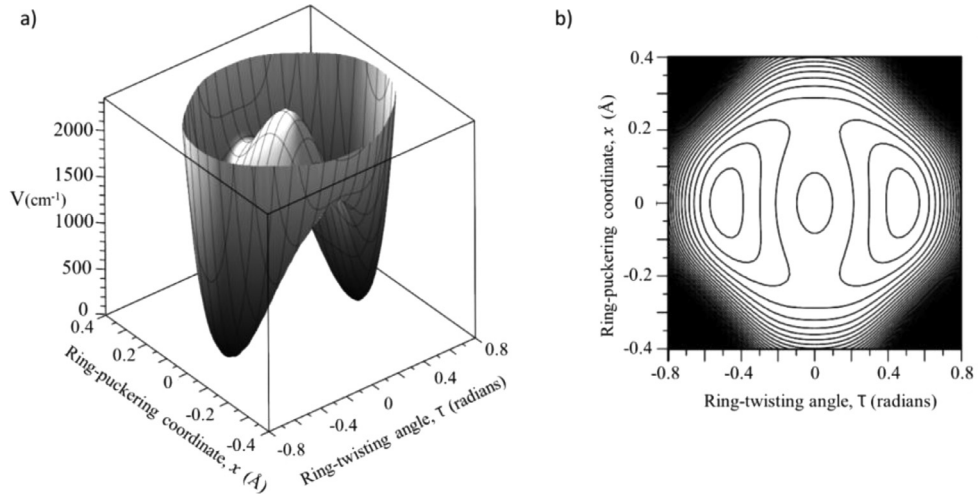

Fig. 7. a) PES and b) contour map for c-$C_4H_8SiF_2$ from MP2/cc-pVTZ computations. The maximum calculated energy corresponds to the planar structure at 2338 cm^{-1}.

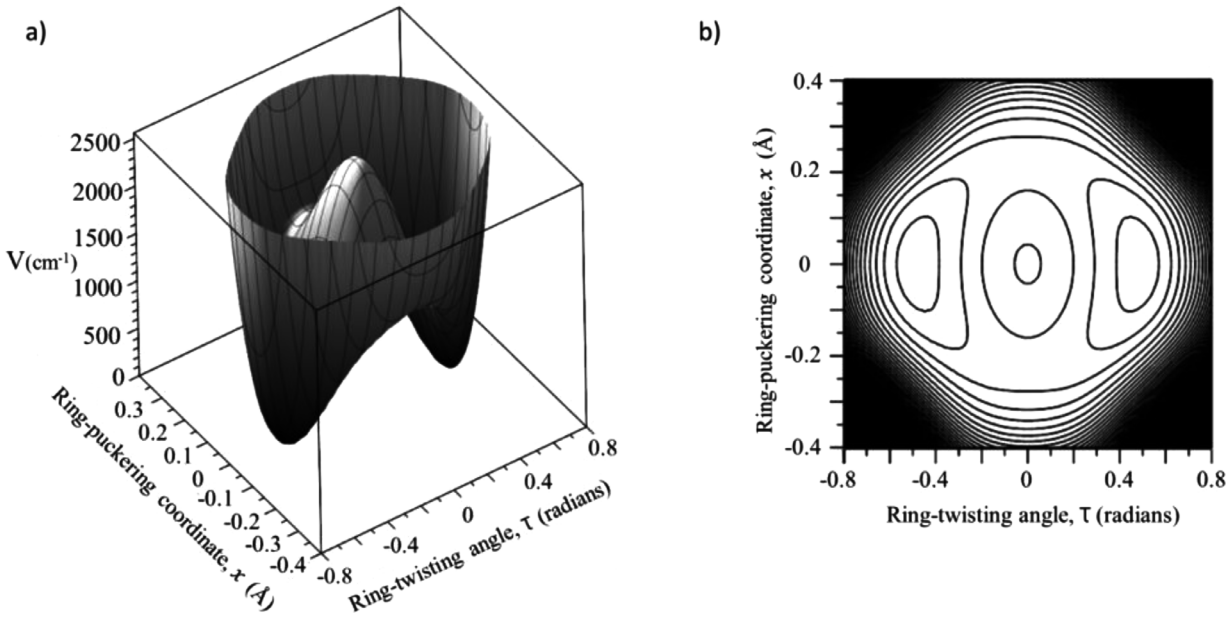

Fig. 8. a) PES and b) contour map for c-$C_4H_8SiH_2$ from MP2/cc-pVTZ computations. The maximum calculated energy corresponds to the planar structure at 2544 cm^{-1}.

required, where F_a is the Coriolis parameter, P_A is the angular momentum about the a-axis, and p_Z is the linear momentum resulting from the inversion moment. This Coriolis parameter has been chosen because the two equivalent structures of c-$C_4H_8SiF_2$ going through the planar maximum energy of the motion arise from the twisting motion about the a-axis. As described by Pickett [38], a better fit of the vibration-rotation interaction results from using the equivalent operator, F_{bc}, $(P_BP_C+P_CP_B)$ p_Z. $\Delta E_{0,1}$ is also necessary to account for the inversion frequency of the ring-twisting motion. Although fitting this type of spectra is described as a tunnelling motion in Pickett, it is fit using vibrational states as labels. Therefore, v = 0 and v = 1 correspond to an A and E of a methyl rotor or + and – of a ring-twisting motion. As a check for self-consistency, two fits were undertaken as noted in Table 5. One is labelled “Fit Separately”, and the other is labelled “Fit Together”. In the “Fit Separately” approach, three rotational constants and three quartic centrifugal distortion constants — D_J, D_{JK}, and D_K — were fit to each individual ring twisting state, labelled v=0 and v=1. In the “Fit Together” approach, only three rotational constants are used with all other constants remaining the same. Both approaches yielded very similar spectroscopic outcomes as shown in Table 5, providing some assurance this was accurately describing the observed splitting. The “Fit Together” approach was used for analysis as that fitting method utilized fewer Hamiltonian parameters with

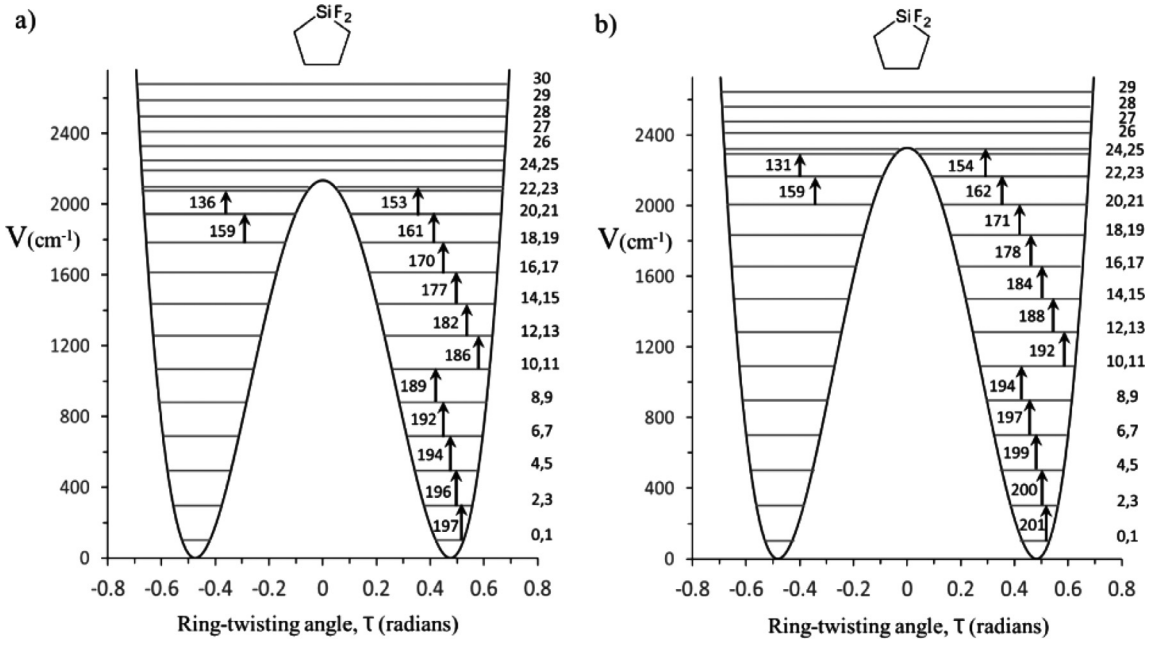

Fig. 9. a) Calculated one-dimensional ring-twisting PEF and energy levels for *c*-$C_4H_8SiF_2$ from CCSD/cc-pVTZ computations (Reduced mass: 33.31 amu). b) Calculated PEF and energy levels for *c*-$C_4H_8SiF_2$ from MP2/cc-pVTZ computations for *c*-$C_4H_8SiF_2$ (Reduced mass: 33.41 amu). All the lowest energy levels in a) and b) appear as degenerate.

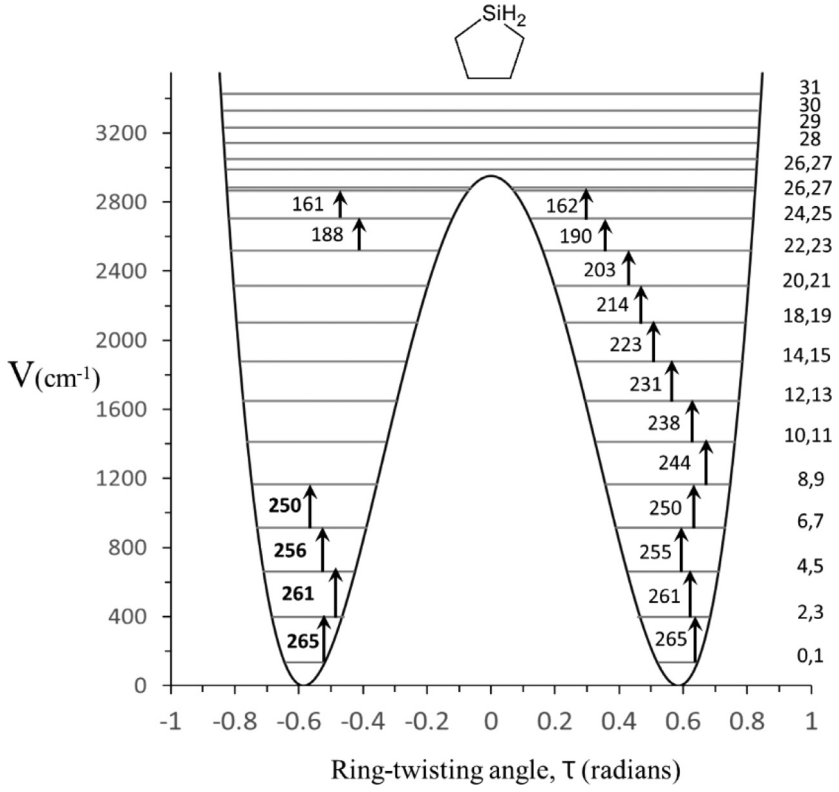

Fig. 10. 1-D PEF from experimental fit for the ring-twisting vibration of *c*-$C_4H_8SiH_2$. The observed values [35] are indicated in bold.

a similar magnitude uncertainty in the fit (within a factor of 2). A list of the split transitions is located in the Supporting Information.

The identification of ^{13}C, ^{29}Si, and ^{30}Si isotopologues was accomplished by obtaining the ratio of the calculated rotational constants of the parent to the experimentally determined ones and using this ratio to adjust the "calculated" isotopologue rotational constants acquired by simply changing the atomic masses of the specific nuclei in question. This yielded isotopologue rotational constant predictions with great accuracy and ease, making traditional assignments for these species much simpler. Then, the correct relative intensity aspect of the CP-FTMW technique was utilized in order to accurately identify each singly substituted species in natural abundance. An example of this relative intensity profile can be found in Fig. 13 for the $5_{15} \leftarrow 4_{14}$ transition. After successfully

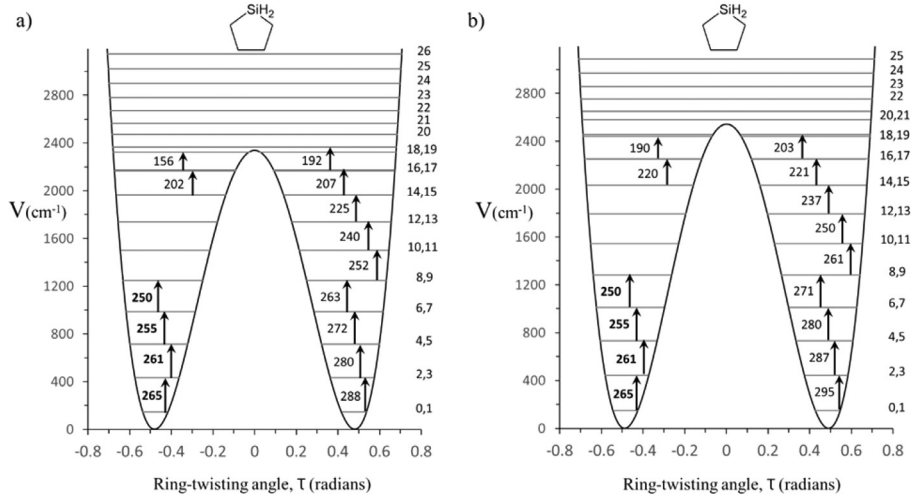

Fig. 11. a) Calculated one-dimensional ring-twisting PEF and energy levels for *c*-$C_4H_8SiH_2$ from CCSD/cc-pVTZ computations (Reduced mass: 33.3 amu). b) Calculated PEF and energy levels for *c*-$C_4H_8SiH_2$ from MP2/cc-pVTZ computations. (Reduced mass: 33.4 amu). All the lowest energy levels in a) and b) appear as degenerated. The observed values [33] are indicated in bold.

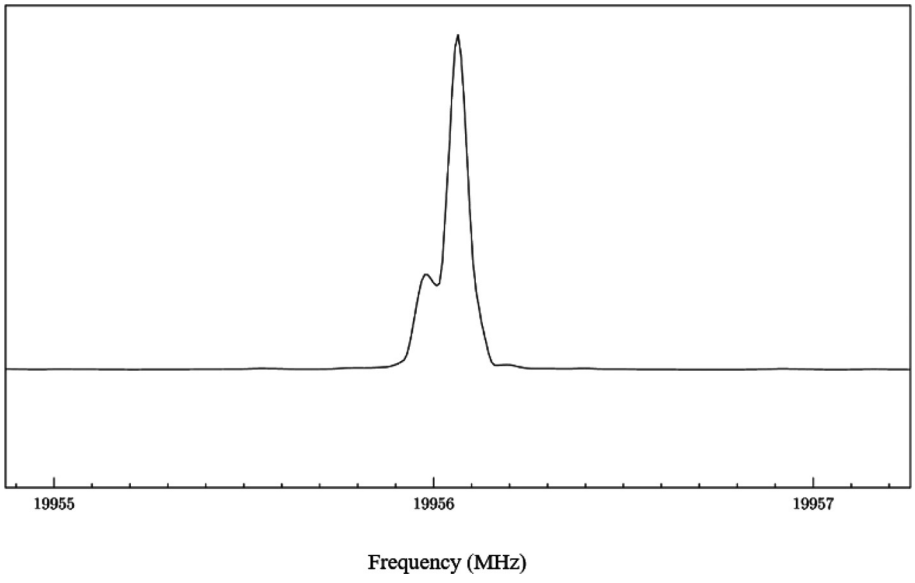

Fig. 12. Example of doubling seen in spectrum due to ring-twisting for the $6_{06} \leftarrow 5_{05}$ transition.

Table 6
Kraitchman Atomic Coordinates[a] with Costain Errors [39].

	^{29}Si (Å)	^{30}Si (Å)	^{13}C1 / ^{13}C4 (Å)	^{13}C2 / ^{13}C3 (Å)[a]
a	0.57 ± 0.11	0.57 ± 0.01	0.62 ± 0.01	2.0 ± 0.01
b	0.00[b] ± 0.10	0.00 ± 0.08	(-/+)[c] 1.3 ± 0.01	(-/+)[d] 0.77 ± 0.01
c	0.00 ± 0.09	0.00 ± 0.07	(+/-)[c] 0.65 ± 0.01	(+/-)[d] 0.03 ± 0.13

[a] Kraitchman Analysis only reports magnitude, but signs of coordinates were assigned by authors to correspond to their computed position values.
[b] Values reported as 0.00 are imaginary values.
[c] The first sign in parentheses represents C1 while the second represents C4.
[d] The first sign in parentheses represents C2 while the second represents C3.

assigning the spectra associated with each isotopologue, a Kraitchman [39] substitution structure for the ring was determined. This process was carried out using Kisiel's KRA program [40]. The results from the Kraitchman analysis can be seen in Table 6. Then, Kisiel's EVAL program [28] was utilized to determine the corresponding bond angles, bond lengths, and dihedral angles for the elements contained within the ring. Both the KRA and EVAL program were obtained from the PROSPE website [40]. Because magnitudes and not absolute atom positions are given in the Kraitchman analysis, experimental structure determinations were aided by substitution of the computational sign values for the experimentally determined positions. From this analysis, the experimental substitution structure for the ring was determined to be nonplanar with a nonzero dihedral angle for every combination in the ring.

5. Discussion

From the results of the high-level *ab initio* calculations and microwave spectroscopy experiments, *c*-$C_4H_8SiF_2$'s minimum energy structure has C_2 symmetry as shown in Fig. 4.

Fig. 14 shows the molecule in the *ab*-, *ac*-, and *bc*-molecular planes. As is shown in this view, the minimum energy C_2 structure distributes the twisted carbons out of the *ab*-molecular plane with their mass now distributed in the *ac*-molecular plane. This is consistent with other works performed previously on members of the silacyclopentane family [7,10]. Inversion splitting due to the ring motion in the molecule was observed and analysed via potential energy calculations described previously. Based on these calcu-

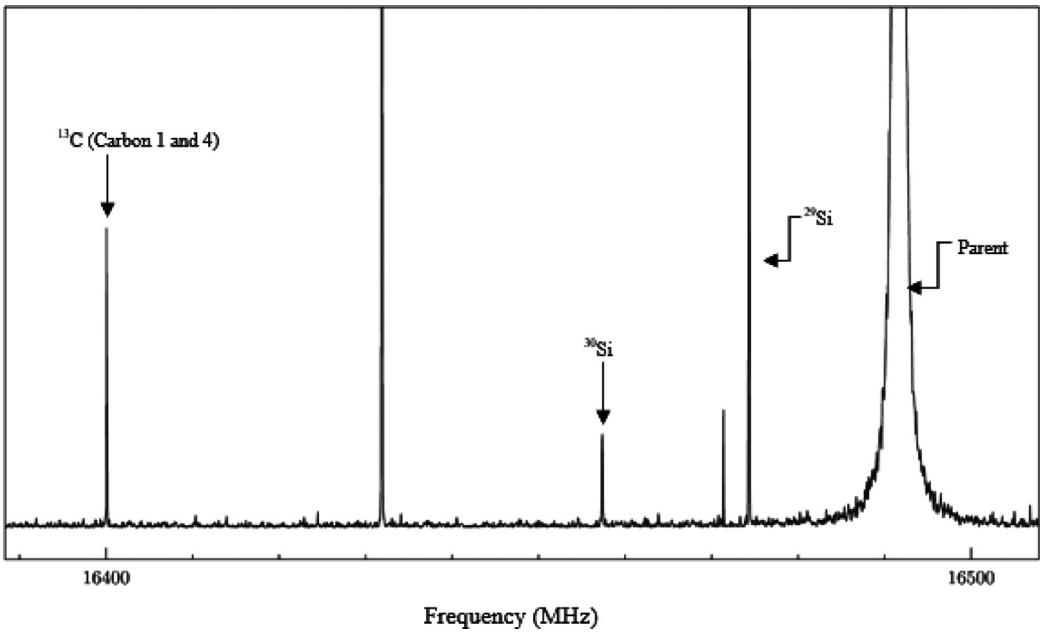

Fig. 13. Example of the relative intensity profile for the isotopic species observed for the $5_{15} \leftarrow 4_{14}$ transition. All species are labeled within the figure.

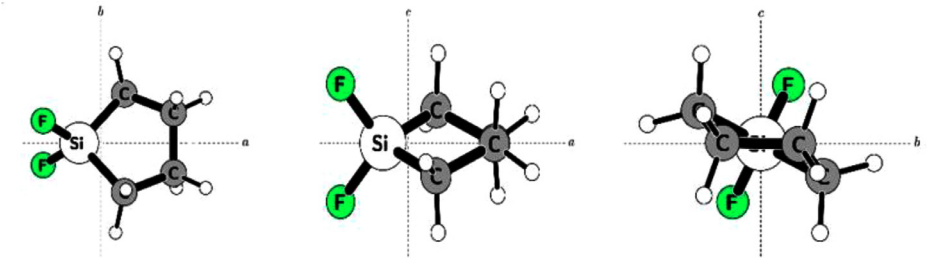

Fig. 14. Calculated geometrical structure of *c*-$C_4H_4SiF_2$ within the *ab*-, *ac*- and *bc*-planes.

Table 7
Second Moment Comparison Between *c*-$C_4H_4SiF_2$ and Related Molecular Species.

	P_{aa} (amu-Å^2)	P_{bb} (amu-Å^2)	P_{cc} (amu-Å^2)
***c*-$C_4H_8SiF_2$**	227.27110(12)	83.037692(12)	67.164670(12)
***c*-$(CH)_2CH_2CH_2SiF_2$[13]**	224.058503(94)	77.698347(94)	62.708151(94)
***c*-$CH_2(CH)_2CH_2SiF_2$[43]**	217.351320(13)	78.740452(13)	63.705230(13)
***c*-C_4H_8SiHF [11]**	185.68(01)	79.82(01)	27.70(01)
***c*-$CH_2(CH)_2CH_2SiH_2$ [43]**	105.135570(77)	78.740452(77)	6.224120(77)
***c*-$C_4H_8SiH_2$ [10]**	109.85388(1)	80.028848(1)	12.35876(1)

lations, it was determined that there are two equal conformations for the minimum energy structure that were separated by an energy barrier corresponding to the planar conformation. The potential energy barrier between these two minimum energy structures, accessible by a ring-twisting motion, is calculated to be 2338 cm^{-1}. From this potential energy surface, the lowest energy levels appear degenerate. There is still enough nondegeneracy, however, at the bottom of the well which has been observed at the resolution of the CP-FTMW experiment. The experimentally determined splitting of these states is approximately 1.33 cm^{-1}, well within the uncertainty of the calculations presented.

In order to understand more regarding the determined structure of *c*-$C_4H_8SiF_2$, it is ideal to compare it to other molecules within the silacyclopentane family. Because second moments measure the extension of a molecule's mass along a given axis (or outside a plane), it provides an efficient way to interpret a molecule's structure, especially when only parent isotopologue data are available [41,42]. Within Table 7, the second moments for six molecules can be seen. In addition to *c*-$C_4H_8SiF_2$, this table includes 1,1-difluoro-1-silacyclopent-2-ene (*c*-$(CH)_2CH_2CH_2SiF_2$) [13], 1,1-difluoro-1-silacyclopent-3-ene (*c*-$CH_2(CH)_2CH_2SiF_2$) [43], 1-fluoro-1-silacyclopentane (*c*-C_4H_8SiHF) [11], silacyclopent-3-ene (*c*-$CH_2(CH)_2CH_2SiH_2$) [43], and finally *c*-$C_4H_8SiH_2$ [10]. The second moments reported in Table 7 were obtained using the PLANM program obtained from PROSPE [40] in conjunction with the rotational constants reported in the respective works. The structures of these molecules can be seen in Fig. 15.

The second moment values presented in Table 7 may provide structural insight [41,42], but care must be taken in order to make comparisons within a family. First of all, halogen substitution will cause a shift in the *a*-, *b*-, and *c*-axis system, so it is easiest to make comparisons among species with equal substitution above and below the ring (difluoro molecules, for example). Because ring-planarity in these molecules moves mass out of the *ab*-plane and into the *ac*-plane, we can monitor planarity by comparison of the

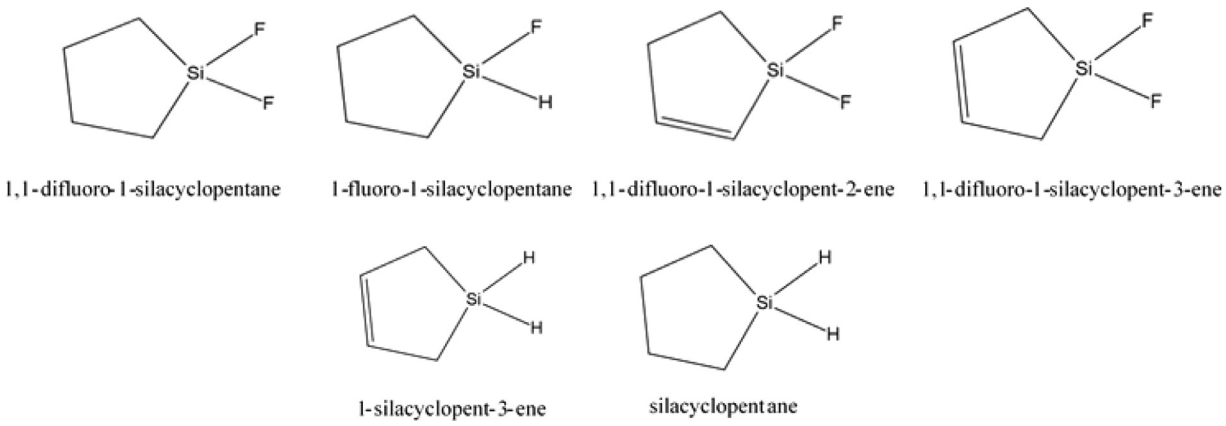

Fig. 15. Molecular structures of molecules under comparison.

P_{bb} (out-of-*ac*-plane mass) and P_{cc} (out-of-*ab*-plane mass) values. We will focus on P_{bb} here because the change in P_{cc} values due to halogenation make them also hard to follow. *c*-$(CH)_2CH_2CH_2SiF_2$, *c*-$CH_2(CH)_2CH_2SiF_2$, and *c*-$CH_2(CH)_2CH_2SiH_2$ are known to be planar [13,43]. Their P_{bb} values all lie within 1.1 amu-Å^2 of one another. The nonplanar molecules, *c*-$C_4H_8SiF_2$ and *c*-$C_4H_8SiH_2$, have an increase in P_{bb} greater than 1.1 amu-Å^2 from any of the comparator planar molecules with an increase of >4 amu-Å^2 for *c*-$C_4H_8SiF_2$. This can only be due to the carbons twisting out of the *ab*-plane and into the *ac*-plane as is shown in Fig. 14.

Another comparison that can be drawn between the six molecules listed in Table 7 is the presence of splitting within the spectra from non-degenerate energy levels present due to ring-twisting. For the work performed on *c*-$C_4H_8SiH_2$ [10], *c*-$(CH)_2CH_2CH_2SiF_2$ [13] and *c*-C_4H_8SiHF [11], no split transitions were reported. However, for *c*-$C_4H_8SiF_2$, *c*-$CH_2(CH)_2CH_2SiF_2$, and *c*-$CH_2(CH)_2CH_2SiH_2$ splitting was observed [43]. Though, it should be noted that the source of the splitting for *c*-$CH_2(CH)_2CH_2SiF_2$ was undetermined. Within the present work, fifteen split transitions were observed and assigned. What is interesting about the specific transitions that exhibited splitting was that they were not from the strongest transitions but from weaker transitions with higher *J* values. These transitions tended to be weaker in intensity in our spectrum, so their observation is due to the deep averaging and resolution capabilities of the CP-FTMW, the molecule's large dipole moment, and smaller rotational constants due to the mass of the molecule. As a result, we hypothesize that the similar molecule *c*-$C_4H_8SiH_2$ should possess split transitions but were not observed because the higher *J* values were not accessible in the experiment.

The evolution of experiments performed on the members of the silacyclopentane family, therefore, is representative of the sensitivity improvements that have been made with the CP-FTMW. The observation of split transitions where there are none predicted within computational uncertainty provides a basis to improve current theoretical approaches so that models may be refined. Yet, the heavy-atom experimental (r_s) structure agrees well with the equilibrium geometry predicted by the theoretical approaches employed indicating that the optimized structures are correct.

6. Summary

Within this work, the pure rotational spectrum of *c*-$C_4H_8SiF_2$ was studied using CP-FTMW. In addition to the parent species, the isotopologues of ^{13}C, ^{29}Si, and ^{30}Si were also measured and fit, resulting in the generation of a heavy atom structure. This structure exhibited ring-twisting that caused certain transitions to appear split. Potential energy surfaces for the ring twisting motion were undertaken and the experimentally determined energy level difference observed in comparison to these surfaces is reasonable. The ring structure of *c*-$C_4H_8SiF_2$ has been determined to be nonplanar through Kraitchman analysis and comparison of the P_{bb} second moment amongst a family of similar molecules.

Declaration of Competing Interest

The authors declare that they have no known competing financial interests or personal relationships that could have appeared to influence the work reported in this paper.

G. S. Grubbs II reports financial support was provided by National Science Foundation. Gamil Guirgis reports equipment, drugs, or supplies was provided by National Science Foundation. Jaan Laane reports financial support and equipment, drugs, or supplies were provided by Welch Foundation.

CRediT authorship contribution statement

Nicole T. Moon: Writing – original draft, Writing – review & editing, Investigation, Formal analysis. **Frank E. Marshall:** Investigation, Formal analysis. **Thomas M.C. McFadden:** Investigation, Formal analysis, Writing – review & editing. **Esther J. Ocola:** Investigation, Formal analysis, Writing – original draft, Writing – review & editing. **Jaan Laane:** Supervision, Formal analysis, Writing – review & editing, Funding acquisition. **Gamil A. Guirgis:** Supervision, Formal analysis, Writing – review & editing, Funding acquisition. **Garry S. Grubbs II:** Supervision, Conceptualization, Investigation, Formal analysis, Writing – original draft, Writing – review & editing, Funding acquisition.

Acknowledgements

Missouri S&T material is based upon work supported by the National Science Foundation under Grant No. CHE-2019072. The NMR spectrometer used in this study at the College of Charleston is supported by the National Science Foundation under Grant No. 1429308. J. Laane and E. J. Ocola wish to thank the Welch Foundation (Grant A-0396) for financial support and the Texas A&M High Performance Research Computing, Texas A&M University, College Station, for computational resources.

Supplementary materials

Supplementary material associated with this article can be found, in the online version, at doi:10.1016/j.molstruc.2021.131563.

References

[1] G.G. Brown, B.C. Dian, K.O. Douglass, S.M. Geyer, S.T. Shipman, B.H. Pate, Rev. Sci. Instrum. 79 (2008) 53103.
[2] T.J. Balle, W.H. Flygare, Rev. Sci. Instrum. 52 (1981) 33.
[3] G.B. Park, R.W. Field, J. Chem. Phys. 144 (2016) 200901.
[4] G.S. Grubbs II, C.T. Dewberry, K.C. Etchison, E.K. Kerr, S.A Cooke, Rev. Sci. Instrum. 78 (2007) 096106.
[5] F.E. Marshall, J.L. Neill, M.T. Muckle, B.H. Pate, Z. Kisiel, G.S. Grubbs, II J.Mol. Spectrosc. 344 (2018) 34–38.
[6] F.E. Marshall, R. Dorris, S.A. Peebles, R.A. Peebles, G.S. Grubbs II, J. Phys. Chem. A 122 (2018) 7385.
[7] J.R. Durig, W.J. Lafferty, V.F. Kalasinsky, J. Phys. Chem. 80 (11) (1976) 1199.
[8] J. Laane, J. Chem. Phys. 50 (1969) 1946.
[9] H.J. Chun, L.F. Colegrove, Laane, J. Chem. Phys. 431 (2014) 15–19.
[10] Z. Chen, J. van Winjgaarden, J. Mol. Spec. 269 (2011) 137–140.
[11] J.R. Durig, S.S. Panikar, B.J. Obenchain, B.J. Bills, P.M. Lohan, R.A. Peebles, S.A. Peebles, P. Groner, G.A. Guirgis, M.D. Johnston, J Chem. Phys. 136 (2012) 044306.
[12] G.A. Guirgis, S.S. Panikar, J.J. Klassen, S.S. Purohit, M.D. Johnston, J.R. Durig, Spectrochimicia Acta Part A 79 (2011) 858–866.
[13] T.M.C. McFadden, F.E. Marshall, E.J. Ocola, J. Laane, G.A. Guirgis, G.S. Grubbs, J. Phys. Chem. A. 124 (2020) 8254–8262.
[14] S. Bell, H.D. Stidham, A.J. LaPlante, Y.Y. Zheng, G.A. Guirgis, J. Mol. Strut. 992 (2011) 1.
[15] J.R. Durig, S.S. Panikar, K.A. Glenn, Y.Y. Zheng, G.A. Guirgis, Vib Spectrosc 55 (2) (2011) 250.
[16] J.R. Durig, M. Johnson-Streusand, J. Raman Spectrosc 9 (1) (1980) 50.
[17] G.A. Guirgis, J.J. Klaassen, B.H. Pate, N.A. Seifert, I.D. Darkhail, B.S. Deodhar, J .K. Wyatt, H.W. Dukes, M. Kruger, J.R. Durig, J. Mol. Struct. 1049 (2013) 400.
[18] J. Ceponkus, V. Savlinskas, V. Aleksa, M. Pucetaite, R. Platakyte, C.W. Reed, C. Cotter, G Guirgis, . Vib. Spectrosc. 81 (2015) 136.
[19] B.H. Pate, N.A. Seifert, G.A. Guirgis, B.S. Deodhar, J.J. Klassen, I.D. Darkhailil, J.A. Crow, J.K. Wyatt, H.W. Dukes, J.R. Durig, Chem. Phys 416 (2013) 33.
[20] J.O. Daiss, C. Burschka, J.S. Mills, J.G. Montana, G.A. Showell, J.B.H. Warneck, R. Tacke, Organometallics (2006) 1188–1198.
[21] S.J. Aspin, S. Taillemaud, P. Cyr, A.B. Charette, Angew. Chem. Int. Ed. 55 (2016) 13833–13837.
[22] E.E. Siefert, S.D. Witt, Y.N. Tang, J. Chem. Soc. Chem Commun. (1981) 217b-218.
[23] F.E. Marshall, D.J. Gillcrist, T.D. Persinger, S. Jaeger, C.C. Hurley, N.E. Shreve, N. Moon, G.S. Grubbs II, J. Mol. Spectrosc. 328 (2016) 59–66.
[24] A. Duerden, F.E. Marshall, N. Moon, C. Swanson, K.M. Donnell, G.S. Grubbs II, J. Mol. Spec. 376 (2021) 111396.
[25] M.J. Frisch, G.W. Trucks, H.B. Schlegel, G.E. Scuseria, M.A. Robb, J.R. Cheeseman, G. Scalmani, V. Barone, G.A. Petersson, H. Nakatsuji, X. Li, M. Caricato, A. Marenich, J. Bloino, B.G. Janesko, R. Gomperts, B. Mennucci, H.P. Hratchian, J.V. Ortiz, A.F. Izmaylov, J.L. Sonnenberg, D. Williams-Young, F. Ding, F. Lipparini, F. Egidi, J. Goings, B. Peng, A. Petrone, T. Henderson, D. Ranasinghe, V.G. Zakrzewski, J. Gao, N. Rega, G. Zheng, W. Liang, M. Hada, M. Ehara, K. Toyota, R. Fukuda, J. Hasegawa, M. Ishida, T. Nakajima, Y. Honda, O. Kitao, H. Nakai, T. Vreven, K. Throssell, J.A. Montgomery Jr., J.E. Peralta, F. Ogliaro, M. Bearpark, J.J. Heyd, E. Brothers, K.N. Kudin, V.N. Staroverov, T. Keith, R. Kobayashi, J. Normand, K. Raghavachari, A. Rendell, J.C. Burant, S.S. Iyengar, J. Tomasi, M. Cossi, J.M. Millam, M. Klene, C. Adamo, R. Cammi, J.W. Ochterski, R.L. Martin, K. Morokuma, O. Farkas, J.B. Foresman, D.J. Fox, Gaussian 09, Revision A.02, Gaussian, Inc., Wallingford CT, 2016.
[26] Dennington, R. D.; Keith, T. A.; Millam, J. M.*GaussView 6.1.1,Graphical Interface*; Semichem Inc.: Shawnee, KS, www.gaussian.com. 2000-2019
[27] M.J. Frisch, G.W. Trucks, H.B. Schlegel, G.E. Scuseria, M.A. Robb, J.R. Cheeseman, G. Scalmani, V. Barone, B. Mennucci, G.A. Petersson, et al., *Gaussian 16*, revision B.01, Gaussian, Inc., Wallingford, CT, 2016.
[28] Z. Kisiel, J. Demaison, et al., in: Spectroscopy from Space, Kluwer Academic Publishers, Dordrecht, 2001, pp. 91–106. Eds.
[29] R.W. Schmude Jr., M.A. Harthcock, M.B. Kelly, J. Laane, J. Mol. Spec. 124 (1987) 369–378.
[30] M.M. Strube, J. Laane, J. Mol. Spec. 129 (1988) 126–139.
[31] M.M.J. Tecklenburg, J. Laane, J. Mol. Spec. 137 (1989) 65–81.
[32] J. Laane, M.A. Harthcock, P.M. Killough, L.E. Bauman, J.M. Cooke, J. Mol. Spec. 91 (1982) 286–299.
[33] N. Meinander, J. Laane, J. Mol. Struct. 569 (2001) 1–24.
[34] Maplesoftware for technical computation, Waterloo Maple Inc, Waterloo, ON, Canada, 2015.
[35] L.F. Colegrove, J.C. Wells, J. Laane, J. Chem. Phys. 93 (1990) 6291–6302.
[36] H.M. Pickett, J. Mol. Spectrosc. 148 (1991) 371–377.
[37] Z. Kisiel, L. Pszczołkowski, I.R. Medvedev, M. Winnewisser, F.C. De Lucia, E. Herbst, J. Mol. Spectrosc. 233 (2005) 231–243.
[38] H.M. Pickett, J. Chem. Phys. 56 (1972) 1715–1723.
[39] C.C. Costain, Trans. Am. Crystallogr. Assoc. 2 (1966) 157.
[40] Institute of Physics, Polish Academy of Sciences Al.Lotnikow 32/46, Warszawa, Poland. http://info.ifpan.edu.pl/~kisiel/prospe.htm (accessed May 26, 2021).
[41] R.K. Bohn, J.A. Montgomery Jr., H.H. Michels, Fournier, J. A. J. Mol. Spec. 325 (2016) 42.
[42] G.S. Grubbs II, D.S. Frank, D.A Obenchain, S.A. Cooke, S.E Novick, J. Mol. Spec. 324 (2016) 1.
[43] F.E. Marshal, Structure Determination of 5 Membered Silane Rings Using Microwave Spectroscopy, International Symposium on Molecular Spectroscopy, University of Illinois, Urbana-Champaign, IL, 19 June 2018 Conference Presentation.